

Asymmetric colliding nuclear matter approach in heavy ion collisions

T. Gaitanos^a, C. Fuchs^b, H. H. Wolter^c

^a*Laboratori Nazionali del Sud INFN, I-95123 Catania, Italy*

^b*Institut für Theoretische Physik der Universität Tübingen, D-72076 Tübingen, Germany*

^c*Dept. für Physik, Universität München, D-85748 Garching, Germany*

The early stage of a heavy ion collision is governed by local non-equilibrium momentum distributions which have been approximated by colliding nuclear matter configurations, i.e. by two Lorentz elongated Fermi ellipsoids. This approach has been extended from the previous assumption of symmetric systems to asymmetric 2-Fermi sphere configurations, i.e. to different densities. This provides a smoother transition from the limiting situation of two interpenetrating currents to an equilibrated system. The model is applied to the dynamical situations of heavy ion collisions at intermediate energies within the framework of relativistic transport (RBUU) calculations. We find that the extended colliding nuclear matter approach is more appropriate to describe collective reaction dynamics in terms of flow observables, in particular, for the elliptic flow at low energies.

Key words: Heavy ion collisions at intermediate energies, non-equilibrium effects, colliding nuclear matter, asymmetric density, collective flow, Dirac-Brueckner-Hartree-Fock.

PACS: 25.75.-q, 25.75.Ld, 21.65.+f

1 Introduction

Heavy ion collisions from Fermi energies up to relativistic energies of 1 – 2 AGeV provide the unique possibility to explore the nuclear matter equation of state (EOS) under extreme conditions of density and temperature in the laboratory [1]. In a hydrodynamical picture the time evolution of such a reaction can be understood in terms of a pressure gradient which builds up in the compressed zone and drives the dynamics. Naively, one therefore expected

to obtain a direct access to the nuclear EOS in the measurement of collective flow observables. However, in fact, the situation is more complex: The system does not behave like an ideal fluid but binary nucleon-nucleon collisions lead to a viscous behavior. Moreover, calculations show that over most of the reaction time, in particular during the compressional phase, the system is out of *local* equilibrium, see e.g. [2]. Also experimental evidence for non-equilibrium in terms of incomplete stopping even in central reactions has recently been reported [3]. Thus the hydrodynamical limit is not reached in relativistic heavy ion reactions except in the final stages of the collision.

On the other hand, microscopic transport models have proved to be an adequate tool for the description of the non-equilibrium reaction dynamics at intermediate energies [1]. The physical input of such semi-classical models based on Boltzmann type equations are the nuclear mean field U and the nucleon-nucleon (NN) cross section σ . Both are derived from the effective two-body interaction in the medium, i.e. the in-medium G-matrix; $U \sim (\Re G\rho)$, $\sigma \sim (\Im G\rho)$, respectively $d\sigma/d\Omega \sim |G|^2$. However, in most practical applications phenomenological mean fields are used. Adjusting the known bulk properties of nuclear matter around saturation one has to rely on extrapolations to supranormal densities. One can then try to constrain the models with the help of heavy ion reactions [4,5].

As mentioned above, in heavy ion collisions the system is far away from local equilibrium even during the high density phase which mainly governs the dynamics of the process. In a fully consistent treatment non-equilibrium effects should be considered self consistently within the framework of microscopic many-body theory and a dynamical description of the reaction, e.g. by Boltzmann type transport equation [6]. An exact solution of the problem would require a consistent treatment of the transport equation and the microscopic structure equations, e.g. within the framework of Dirac-Brueckner (DB) theory, for general non-equilibrium situations. Thus one would have to determine the relativistic in-medium G-matrix not only for an equilibrated Fermi sphere, but for arbitrary momentum distributions, in principle also at finite temperatures. This is presently not possible without introducing further approximations. The simplest approximation is the Local Density Approximation (LDA), which assumes a local spherical, sharp Fermi sphere, and thus essentially neglects non-equilibrium effects in the in-medium interactions. As a step towards non-equilibrium the Colliding Nuclear Matter (CNM) model [7] was introduced (which was also called the Local phase space Configuration Approximation, LCA), which parametrizes the local momentum distribution by two Fermi spheres with a finite relative velocity. We have shown previously that the non-equilibrium effects included in the CNM model modify the underlying EOS, in particular, the dynamical EOS effectively *seen* during a heavy ion collision is softened compared to ground state matter at equivalent densities [8]. This affects the collective dynamics, e.g. in terms of observable

flow signals [9,10]. From these studies it was concluded that this type of non-equilibrium features should be included at the mean-field level in transport analysis of heavy ion reactions in order to allow more reliable conclusions on the nuclear matter EOS.

The Colliding Nuclear Matter (CNM) model has been extensively studied in [7] and has been applied to intermediate energy heavy ion collisions in refs. [8–10]. There it was shown that the consideration of non-equilibrium effects within the CNM approach essentially changes the description of collective dynamics relative to a treatment in the local density approximation (LDA). Differences of the two approximations appeared in collective flow observables and were found to be of the same magnitude as those which arise due to a different, i.e. soft or a hard, EOS.

In this work we extend our previous studies by including more details in the approximations involved in the description of non-equilibrium situations within the CNM approach. In previous applications a symmetric configuration was assumed, i.e. two nuclear matter streams of equal (averaged) density. This should not be very realistic, particularly in peripheral collisions. For this purpose the Asymmetric Colliding Nuclear Matter (ACNM) model is introduced here, which accounts also for a possible asymmetry of the Fermi momenta of the two Fermi fluids. This situation arises in those regions where the tail of one nucleus penetrates into the interior of the other (see e.g. Fig. 1). In previous studies based on the CNM approximation we mainly considered symmetric colliding systems. A locally asymmetric two-stream situation is also more frequently encountered in collisions of different mass systems. Such reactions will experimentally be studied more often in the future. Thus the extended approximation is a further step into the direction of ref. [6], i.e. the attempt to describe the complex dynamical situation in heavy ion reactions as precisely as possible. The extension to ACNM is found to be particularly important at low and intermediate energies when peripheral heavy ion collisions are considered.

2 Approximations in colliding nuclear matter

As discussed in the introduction the treatment of non-equilibrium effects in dynamical transport descriptions cannot be done without any approximations due to its high complexity. In the CNM approach [7] ground state DB results are extrapolated for idealized 2-Fermi spheres or, covariantly, for 2-Fermi ellipsoids, at zero temperature. This approximation constructs the 2-Fermi sphere configuration in a covariantly consistent way with respect to the effective masses, but neglects the blocking in the intermediate propagator due to the second current. It was shown in [7] that this approximation is reliable due to a moderate dependence of the DB self energy around the Fermi momentum.

In applications to heavy ion reactions the relevant approximations are (a) the zero-temperature limit and (b) the restriction to symmetric CNM distributions, i.e. same Fermi momenta of the two counter-streaming currents. To demonstrate these effects we show in Fig. 1 typical local momentum distributions as they are obtained from transport descriptions of central Au+Au reaction at 0.6 AGeV beam energy at different locations in coordinate space (in the center of mass, and in beam direction) at the time just before the compression phase. In the left column we show the local momentum distributions as they are obtained from relativistic BUU calculations. Details of the RBUU model used here are given in section 4. In the right column are asymmetric fits to the momentum distribution, i.e. fits with two Fermi distributions (including Pauli corrections) of different density and temperature, for details see [2]. It is seen from these fits that the momentum space consists in general of two rather different Fermi distributions outside of the central cell, which are furthermore characterized by different local temperatures of the subsystems.

How to go beyond the zero-temperature approximation is difficult to study. The DB approach [11,12] has been mainly applied for ground state nuclear matter at zero temperature. The few existing finite temperature calculations indicate a moderate T -dependence of the mean field at temperatures of a several MeV [11]. Thus, one can expect that the approximation should be reliable for small thermal excitations with moderate momentum tails. In heavy ion collisions high thermal excitations with local temperatures of $T \sim 20 - 40$ MeV in the central region during the compression phase can be reached at intermediate energies, (see Fig. 1), which makes this approximation less obvious. However, we believe that temperature effects become important in a higher order correction and, in addition, complicate the calculation significantly. The determination of a local temperature in heavy ion collisions, which is necessary for such a treatment, requires a fit procedure at each space-time point. Thus, we do not consider a possible temperature dependence of the mean field here.

The assumption of a symmetric CNM approximation should be reliable for central collisions and high beam energies. However, as seen in Fig. 1 this is not the case especially if one goes away from the central cell. We expect the asymmetry of the CNM configuration to be particularly important at low energies. At high energies, on the other side, faster time scales and a higher transparency of the system - for peripheral reactions - leads rather to a separation between 2- and 1-Fermi sphere configurations. Thus, we extend the CNM model to asymmetric 2-Fermi ellipsoid situations (called as Asymmetric Colliding Nuclear Matter (ACNM) in the following).

3 Asymmetric colliding nuclear matter in the relativistic DB approach

The treatment of non-equilibrium effects within the spirit of a CNM approximation has been extensively investigated in ref. [7]. Here we extend this approach to Asymmetric Colliding Nuclear Matter (ACNM) by introducing an asymmetry in the Fermi momenta of the two counter-streaming systems. We describe the idea of the formalism here; more detail can be found in ref. [7].

The momentum distributions are described in terms of a superposition of two counter-streaming nuclear matter currents, i.e. two boosted Fermi ellipsoids at zero temperature. This configuration is schematically shown in Fig. 2. Analytically we write it as

$$f_{12}(\mathbf{k}) = f_1(\mathbf{k}, k_{F_1}) + f_2(\mathbf{k}, k_{F_2}) + \delta f(\mathbf{k}) \\ = \Theta(\mu_1^* - k_\mu u_1^\mu) + \Theta(\mu_2^* - k_\mu u_2^\mu) + \delta f(\mathbf{k}^*) \quad . \quad (1)$$

Θ is the step function, k_{F_i} ($i=1,2$) are the Fermi momenta and $u_i^\nu = (\gamma_i, \mathbf{u}_i \gamma_i)$ are the streaming four velocities of the two boosted nuclear matter currents. The chemical potentials in the moving system are then given as

$$\mu_i(k) = \mu_i^*(k) + \Sigma_\alpha u_i^\alpha = \sqrt{k_{F_i}^2 + m^{*2}} + \Sigma_\alpha u_i^\alpha$$

in terms of the effective chemical potentials $\mu_i^*(k)$ in the rest system. The last term in eq. (1) $\delta f(\mathbf{k})$ guarantees the conservation of the Pauli principle in the overlap region between the two nuclear matter currents, and it is given by $\delta f(\mathbf{k}) = -\Theta_1(\mathbf{k})\Theta_2(\mathbf{k})$. However, to guarantee baryon number conservation one has to restore the total baryon density. This can be done in a covariant manner by redefining the Fermi momenta [7].

The ACNM configuration is characterized by three invariant parameters, the invariant densities of the two Fermi ellipsoids and the relative velocity

$$\rho_i = \sqrt{j_{i\mu} j_i^\mu} \quad , \quad v_{\text{rel}} = \left| \frac{\mathbf{v}_1 - \mathbf{v}_2}{1 - \mathbf{v}_1 \cdot \mathbf{v}_2} \right| \quad . \quad (2)$$

An alternate set of configuration parameters, denoted collectively by χ , are $\chi = \{v_{\text{rel}}, \rho_{\text{tot}}, \rho_\delta\}$ where $\rho_{\text{tot}} = \rho_1 + \rho_2$ is the total invariant density, and

$$\rho_\delta = \frac{\rho_1 - \rho_2}{\rho_{\text{tot}}} \quad (3)$$

the density asymmetry parameter. $\rho_\delta = 0$ corresponds to the special cases of symmetric CNM, $\rho_\delta = 1$ to a single Fermi-sphere at rest with invariant

density $\rho_1 = \rho_{\text{tot}}$ and a single nucleon with relative velocity v_{rel} . Thus, the ACNM model naturally includes a smooth transition to the local density approximation (LDA) of equilibrated nuclear matter for both cases $v_{\text{rel}} \mapsto 0$ and $\rho_\delta \mapsto 0$ while symmetric colliding nuclear matter contains only the first limit. All the expressions for the scalar and baryon densities can be derived in terms of these invariants.

The relativistic self-energy in CNM as well as in ACNM has the same Lorentz structure as in ground state matter, i.e. it contains a scalar part entering into the effective mass m^* and a vector part entering into the kinetic four-momentum k_μ^* [7,8]

$$\Sigma(k) = \Sigma_S(k) - \gamma_\mu \Sigma^\mu(k) \quad . \quad (4)$$

The construction of ACNM is done in a manifestly covariant way and it can be defined in any reference frame. It is, however, most appropriate to work locally in that frame where the total baryon current vanishes $\mathbf{j}_{12} = \mathbf{j}_1 + \mathbf{j}_2 = \mathbf{0}$. We will denote it as current-zero frame RS_{12} in the following and we will work always in RS_{12} . The space-like part of the vector field vanishes in RS_{12} by definition $\Sigma_{12} = \Sigma_1 + \Sigma_2 = \mathbf{0}$ and $\mathbf{k}^* = \mathbf{k}$. This simplifies the situation considerably, since canonical and kinetic momenta are not identical in general frames.

As discussed above, we construct ACNM by extrapolating from calculations of ground state nuclear matter in the DB approach. The self-energies are thereby given as

$$\Sigma_m(k; k_F) = \mathcal{C} \int d^3q g_m(|\mathbf{q}|) f(\mathbf{q}; k_F) \mathcal{T}_m(k, q) \quad (5)$$

in terms of the distribution function $f(\mathbf{q}; k_F)$ of one Fermi sphere ($\mathcal{C} \equiv \frac{\kappa}{(2\pi)^3}$ with $\kappa = 4$ for nuclear matter). Here $m = s, 0$ stands for scalar and (time component) vector self-energies. The \mathcal{T} matrix amplitudes can be taken from DB calculations and g_m in (8) are appropriate weight factors corresponding to the Lorentz structure of these amplitudes [7,8]. The invariant \mathcal{T} matrix amplitudes themselves are determined in equilibrated nuclear matter, i.e. for a single Fermi sphere. We further define effective coupling functions as

$$\Gamma_m = \Sigma_m / \rho_m \quad . \quad (6)$$

In Relativistic Mean Field (RMF) theory these quantities correspond to g_m^2/m_m^2 , where g_m are the coupling constants of the m -meson to the nucleon and m_m its mass.

The ACNM self-energies are given in a corresponding way by using the ACNM distribution function of eq. (1) for a configuration specified by the parameters $\chi = \{v_{\text{rel}}, \rho_{\text{tot}}, \rho_\delta\}$

$$\begin{aligned}\Sigma_m^{(12)}(k; \chi) &= \mathcal{C} \int d^3q g_m(|\mathbf{q}|) f_{12}(\mathbf{q}; \chi) \mathcal{T}_m(k, q, \chi) \\ &= \Sigma_m^{(1)}(k; \chi) + \Sigma_m^{(2)}(k; \chi) + \delta\Sigma_m(k; \chi) \quad .\end{aligned}\quad (7)$$

In the second line it is written as a sum of contributions of two streaming Fermi spheres and a Pauli correction. Note, that the effective \mathcal{T} matrix also depends on the configuration parameters, since the intermediate propagator does. In the first two terms the self energies for the two streaming nuclear matters are specified as (i=1,2)

$$\begin{aligned}\Sigma_m^{(i)}(k; \chi) &= \mathcal{C} \int d^3q g_m(|\mathbf{q}|) f_i(\mathbf{q}; \chi) \mathcal{T}_m(k, q, \chi) \\ &\simeq \Gamma_m(\Lambda^{-1}k; k_F) \rho_m^{(i)}(\chi) \quad .\end{aligned}\quad (8)$$

The second line contains the essential approximation of the approach, namely that the coupling function of ground state nuclear matter are used at momenta corresponding to the appropriate Lorentz boost multiplied by the density of the ACNM configuration. The Pauli correction can be evaluated in a similar way. Since the fields are only moderately momentum dependent below the Fermi surface, the coupling functions can be determined by evaluating at the Fermi momentum. For the special case of symmetric matter (CNM, $k_{F_1} = k_{F_2} \equiv k_F$) one obtains

$$\begin{aligned}\delta\Sigma_m(k; \chi) &= \mathcal{C} \int d^3q g_m(|\mathbf{q}|) \mathcal{T}_m(k, q) \delta f(q; \chi) = \Gamma_m(k_F, k) \delta\rho_m(\chi) \\ &\approx \Gamma_m(k_F, k_F) \delta\rho_m(\chi) \quad .\end{aligned}\quad (9)$$

In this form all the self energies depend on the variables $\{k; \chi\} = \{k; v_{\text{rel}}, \rho_{\text{tot}}, \rho_\delta\}$. They are difficult to handle in a transport calculation, in particular because of the explicit momentum dependence. In analogy to the Hartree (or RMF) approximation we want to obtain momentum-independent self energies. These are obtained by averaging over the momentum of the ACNM configuration

$$\bar{\Sigma}_m^{(12)}(\chi) = \frac{\int d^3k g_m(|\mathbf{q}|) \Sigma_m^{(12)}(k, \chi) f_{12}(\mathbf{k}, \chi)}{\int d^3k g_m(|\mathbf{q}|) f_{12}(\mathbf{k}, \chi)} \equiv \bar{\Gamma}_m^{(12)}(\chi) \rho_m^{(12)}(\chi) \quad , \quad (10)$$

where analogously as in eq. (6) ACNM coupling functions are defined in the second equality. Details of the averaging procedure and the calculation of the coupling functions are given in the Appendix.

Fig. 3 shows the density asymmetry dependence of the effective coupling functions $\bar{\Gamma}_{s,0}^{(12)}$ (see Eq. (10)) at fixed relative velocity and total densities (solid circles). It is seen that the effective couplings rise with increasing asymmetry ρ_δ and approach the LDA limit.

At high relative velocities and moderate densities, where Pauli effects are only of minor importance, a rising asymmetry parameter shifts the center-of-mass towards the current with the higher density and the mean field is dominated by the momentum distribution of this ellipsoid. Thus, in averaging over the explicit momentum dependence of the fields, mainly moderate relative momenta contribute to the ACNM self energy. On the other hand, the invariants $\mathcal{T}_{s,0}$ increase with decreasing momentum which leads finally to the observed ρ_δ dependence of the Fig. 3. This behavior is more pronounced at larger densities since there the variation of the underlying T-matrix amplitudes is stronger.

The ACNM mean field depends on three parameters which complicates their application in transport calculations for heavy ion collisions. For practical use we apply therefore a simple parameterization of the form ($U(\rho, v_{\text{rel}}, \delta)$ stands for scalar and vector self energies)

$$U^{ACNM} \equiv U(\rho, v_{\text{rel}}, \rho_\delta) = \rho_\delta^2 U^{LDA}(\rho) + (1 - \rho_\delta^2) U^{CNM}(\rho, v_{\text{rel}}) . \quad (11)$$

This parameterization is also shown in Fig. 3 (solid lines). It is sufficiently accurate to be used in heavy ion collisions.

4 Application to heavy ion collisions

For the theoretical description of heavy ion collisions we use the relativistic Boltzmann-Uehling-Uhlenbeck (RBUU) transport equation [6,10]. The mean field will be implemented in three approximations as discussed in the previous section: The symmetric CNM model has been studied in detail previously [9,10], its extension in the ACNM approach based on the parameterization (11) is studied here for the first time. Results are also compared to the LDA where the mean field is only a function of the total density, i.e. taken at zero relative velocity $v_{\text{rel}} = 0$. The density and momentum dependence of the mean field is taken from the DB model of Ref. [12]. The nuclear matter saturation properties obtained with the Bonn A potential are $\rho_{\text{sat}} = 0.185 \text{ fm}^{-3}$ and $E = -16.1 \text{ MeV}$. With a compression modulus $K = 230 \text{ MeV}$ one has a relatively soft EOS. In this context one should keep note that the consideration of the non-equilibrium effects in the CNM/ACNM approaches weakens the nucleon effective interaction leading to an even softer EOS than that given in the LDA. In all the simulations the collision integral is treated in

the same way by using standard parameterizations for the elastic and inelastic total and differential cross sections [13] including Δ and N^* resonances. The resonances are propagated in the same mean field as the nucleons and they decay into one and two-pion final channels. The pions are propagated under the influence of the Coulomb interaction. However, they interact strongly with the hadronic environment due to absorption.

We have analyzed Au+Au collisions at intermediate energies in terms of collective flow effects given by its in-plane and out-of-plane components. They can be characterized by the first and second order Fourier coefficients of the azimuthal distributions, $N(\phi) \sim 1 + v_1 \cos(\phi) + 2v_2 \cos(2\phi) + \dots$, and calculated as

$$v_1 = \left\langle \frac{p_x^2}{(p_x^2 + p_y^2)^{1/2}} \right\rangle \quad , \quad v_2 = \left\langle \frac{p_x^2 - p_y^2}{p_x^2 + p_y^2} \right\rangle \quad . \quad (12)$$

In general, $v_{1,2}$ depend, apart from the beam energy and centrality, on rapidity and transverse momentum. This has been studied extensively experimentally, e.g., in refs. [1,14], and theoretically using non-relativistic approaches for the mean field in [4,5,15–18], and relativistically in [9,10,19] and [20] where in the latter case it was claimed to see a softening of the nuclear EOS as nuclear density becomes large.

We begin the flow analysis by discussing the rapidity and transverse momentum dependence of the in-plane flow v_1 in the Figs. 4,5 for semi-central and peripheral Au+Au reactions at 0.25 and 0.4 AGeV. For a realistic simulation of the experimental conditions the RBUU events were passed through a phase space fragment coalescence algorithm including a reaction plane determination in the same way as the FOPI experiment [21,22]. The centrality selection was performed using the total multiplicity of charged particles, see e.g. [10].

From these figures it can be seen that the non-equilibrium effects accounted by the ACNM and CNM models influence the directed in-plane flow only moderately. The differences are relatively biggest at large transverse momenta $p_t^{(0)}$ and in the high rapidity regions. This is expected, since high $p_t^{(0)}$ particles are mainly emitted earlier when the matter is still anisotropic. Mostly, the in-plane flow with ACNM mean fields lies between the CNM and LDA results. This result is to be expected since ACNM interpolates the self-energies between the two extreme cases, CNM and LDA. The different flow pattern originate from the treatment of momentum anisotropies on the mean field level. The momentum dependence included in the CNM and ACNM approximation generally weakens the repulsive vector self energy, in particular at high incident energies, which leads to an effectively softer EOS compared to the nuclear matter EOS (LDA case) [8]. This mechanism reduces the in-plane flow.

The differences become more pronounced for the elliptic flow shown in Figs. 6,7. The elliptic flow is generally considered as a suitable tool to study the momentum dependence of the nuclear mean field [14,4,25]. The elliptic flow is created during the high compression phase and governed by the pressure gradient due to the expansion of the initially compressed fireball as well as by shadowing effects of the spectator matter. Since the high density phase of the collision is still governed by local non-equilibrium [8] one expects to see clear differences between the CNM, ACNM and LDA models. The model dependencies are most pronounced in the transverse momentum dependence of the elliptic flow (Fig. 6). The energy dependence of the $p_t^{(0)}$ integrated elliptic flow (Fig. 7) shows also clear signals from the highly anisotropic compression phase. The LDA yields a very strong elliptic flow and fails to describe the excitation function above 0.25 AGeV. The CNM approximation, on the other hand, reduces the flow, particularly, at high energies and provides a good fit to the data there, but is too small at low energies. At low energies the ACNM model lies between the two limiting cases, LDA and CNM, which results in a rather accurate description of the excitation function over the complete energy range from 0.1 \div 4 AGeV.

The differences between LDA, CNM, and ACNM approaches have the same origin as for the in-plane flow although the model dependencies are now more pronounced. Accounting for momentum anisotropies on the mean field level the repulsion of the model is weakened. Thus, due to the smaller pressure gradients the initially compressed system expands slower which effectively reduces the shadowing effect of spectator matter and the magnitude of the out-of-plane emission. The differences between CNM and ACNM can be understood from Fig. 3. We also find that the asymmetry dependence is similar at other relative velocities and densities not shown here. The increase of the vector field with asymmetry parameter ρ_δ result in a stronger elliptic flow in ACNM as compared to CNM, but still smaller with respect to LDA, as expected. One obtains a smoother transition to LDA as the beam energy decreases.

5 Summary and conclusions

We studied heavy ion collisions with a relativistic transport model and focused on non-equilibrium features of the phase space and their correlation to collective dynamics in terms of flow signals. The non-equilibrium effects were described by a Colliding Nuclear Matter model. We extended this model to two Fermi ellipsoids with an asymmetry in their densities, called as ACNM. The application of CNM and ACNM at intermediate energy heavy ion collisions was compared to a simple Local Density Approximation (LDA).

We analyzed collective flow effects in and out of the reaction plane. It was

found that the directed in-plane flow is only moderately affected by asymmetry effects in the ACNM approach, except if one considers the transverse momentum dependence at high p_t . For high energetic particles the ACNM model provided the best description of the data especially at the lowest bombarding energy considered (0.25 AGeV).

The elliptic flow excitation function is more sensitive to these different approaches since this observable is built during the early non-equilibrium stage of the collision. We observed a reduction of the elliptic flow in the ACNM and CNM models compared to LDA, where the ACNM model gave the best description of the data at intermediate energies. The asymmetry of the configuration was found to be particularly important at low energies and provided a smoother transition to the LDA.

We interpreted the results by the fact that the repulsive vector field is essentially reduced in the CNM and ACNM cases which also decrease the magnitude of flows as compared to LDA. This considerably improves the comparison with flow data. The deviations between CNM and experiment especially at low energies in the elliptic flow excitation function seems to be resolved when asymmetric CNM configurations are considered (ACNM) where a smoother transition to the LDA case is now observed.

We conclude that non-equilibrium effects are important describing the collective dynamics of intermediate energy heavy ion collisions. A fully consistent treatment of heavy ion dynamics and nuclear structure equations within the framework of non-equilibrium transport theory is presently not possible. The CNM/ACNM models provide an approximative, but solvable tool to incorporate local non-equilibrium features more consistently at the level of the effective interaction. For definitive conclusions on the nuclear matter EOS it is important to study such approximations in complex systems. Our results can be considered as a first step in this direction. The next step would be to consider finite temperature effects, as well as the explicit momentum dependence of the fields.

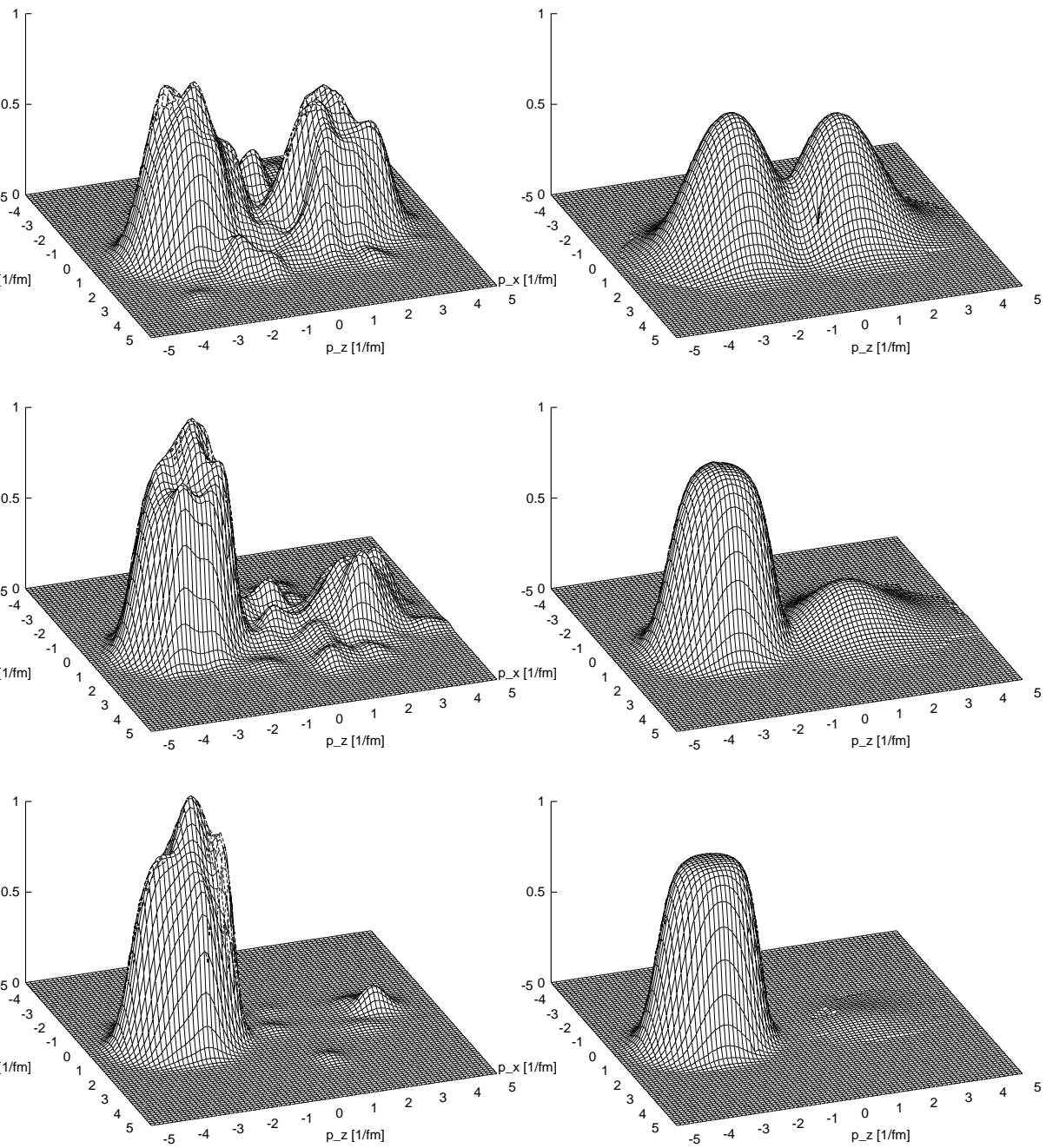


Fig. 1. Left: Local momentum distributions from RBUU at positions $\mathbf{x} = (x, y, z) = (0, 0, 0)$ (top), $\mathbf{x} = (0, 0, 2)$ (middle) and $\mathbf{x} = (0, 0, 4)$ (bottom) (in units of [fm]) at time $t = 10$ fm/c. The figures on the right give the corresponding ACNM momentum distributions at finite temperatures $T_{1,2}$ with values of $T_{1,2} = 29$ MeV (top), $T_1 = 40$ and $T_2 = 8$ MeV (middle) and $T_1 = 25$ und $T_2 = 1$ (bottom). The considered reaction is a central ($b = 0$ fm) Au+Au reaction at $E_{beam} = 600$ AMeV beam energy.

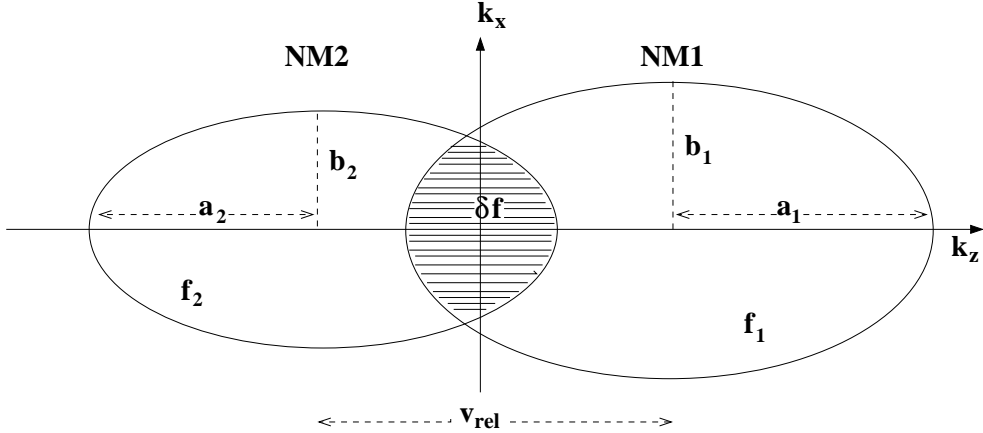


Fig. 2. Schematic representation of the ACNM configuration given by two covariant Fermi ellipsoidal momentum distributions f_i , ($i=1,2$). These are characterized by Fermi momenta ($b_i = k_{F_i}$) which are elongated along the boost direction ($a_i = \gamma_i v_i k_{F_i}$).

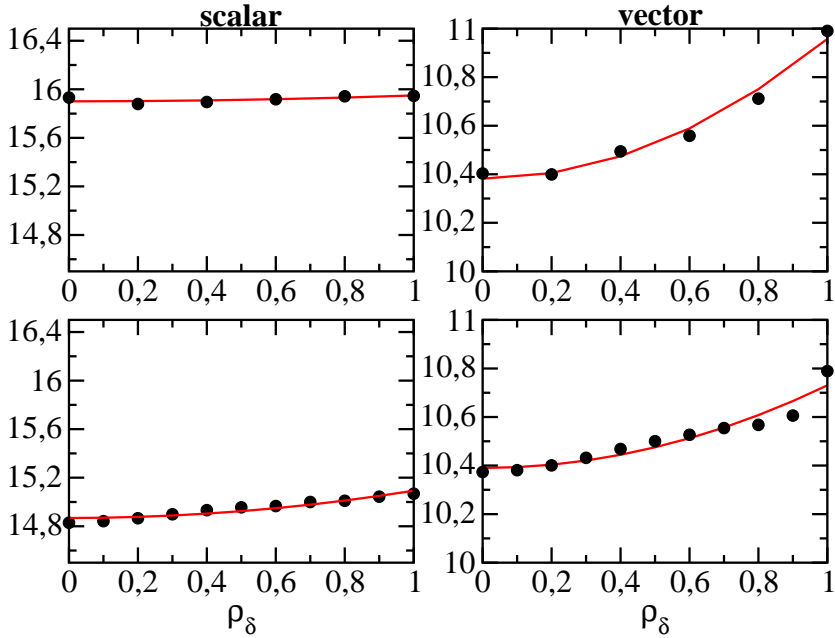


Fig. 3. Effective coupling functions $\bar{\Gamma}_{s,0}^{(12)}$ (left and right figures respectively) as function of the asymmetry parameter ρ_δ at fixed total densities of $\rho_{\text{tot}} = 1$ [ρ_{sat}] (top) and $\rho_{\text{tot}} = 2$ [ρ_{sat}] (bottom) and relative velocity $v_{\text{rel}} = 0.5$ [c]. The circles are results of ACNM calculations and the solid lines indicate the parameterization of Eq. (11).

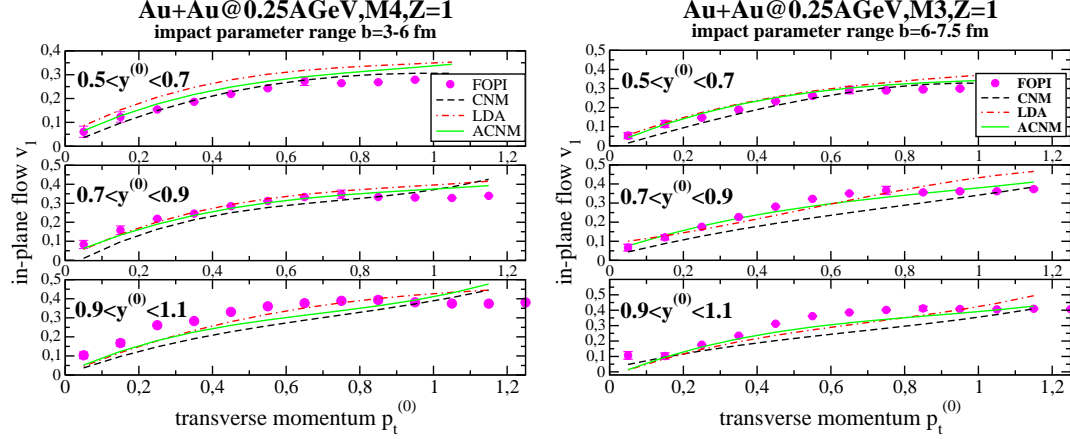


Fig. 4. In-plane collective flow v_1 for charged ($Z = 1$) particles in Au+Au reactions at 0.25 AGeV incident energy as function of the normalized transverse momentum $p_t^{(0)}$ at different rapidity intervals. The centrality intervals M4 and M3 corresponds to impact parameter ranges of (3 – 6 fm) and (6 – 7.5 fm), respectively. RBUU calculations treat the mean field in the following approximations: local density approximation (LDA) where no configuration dependence is included (dot-dashed lines); colliding nuclear matter (CNM) approximation (dashed lines); asymmetric colliding nuclear matter (ACNM) approximation (solid lines). The FOPI data (filled circles) are taken from [22].

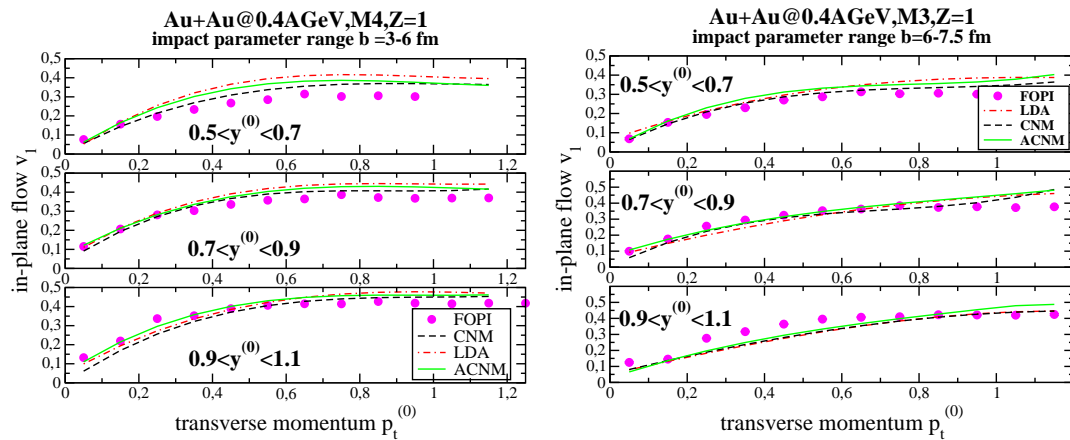


Fig. 5. Same as in Fig. 4, but at 0.4 AGeV incident energy.

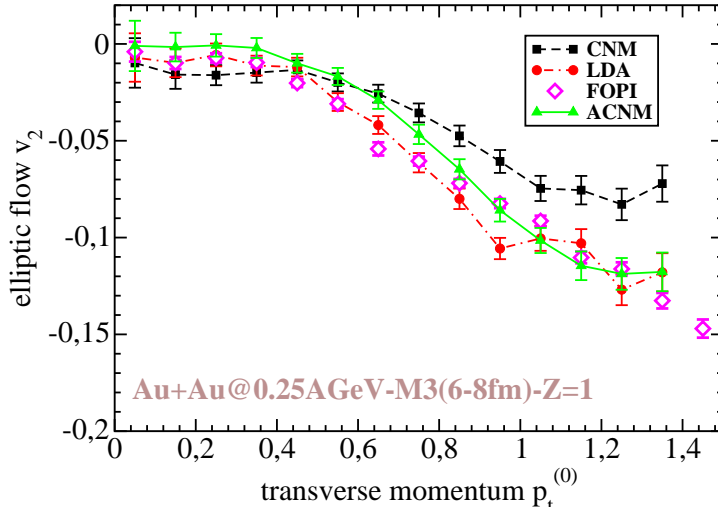


Fig. 6. Out-of-plane collective flow v_2 for charged ($Z = 1$) particles as function of the normalized transverse momentum $p_t^{(0)}$ at mid rapidity $-0.15 \leq y^{(0)} \leq 0.15$ for the reactions as indicated. The models are the same as in Fig. 4.

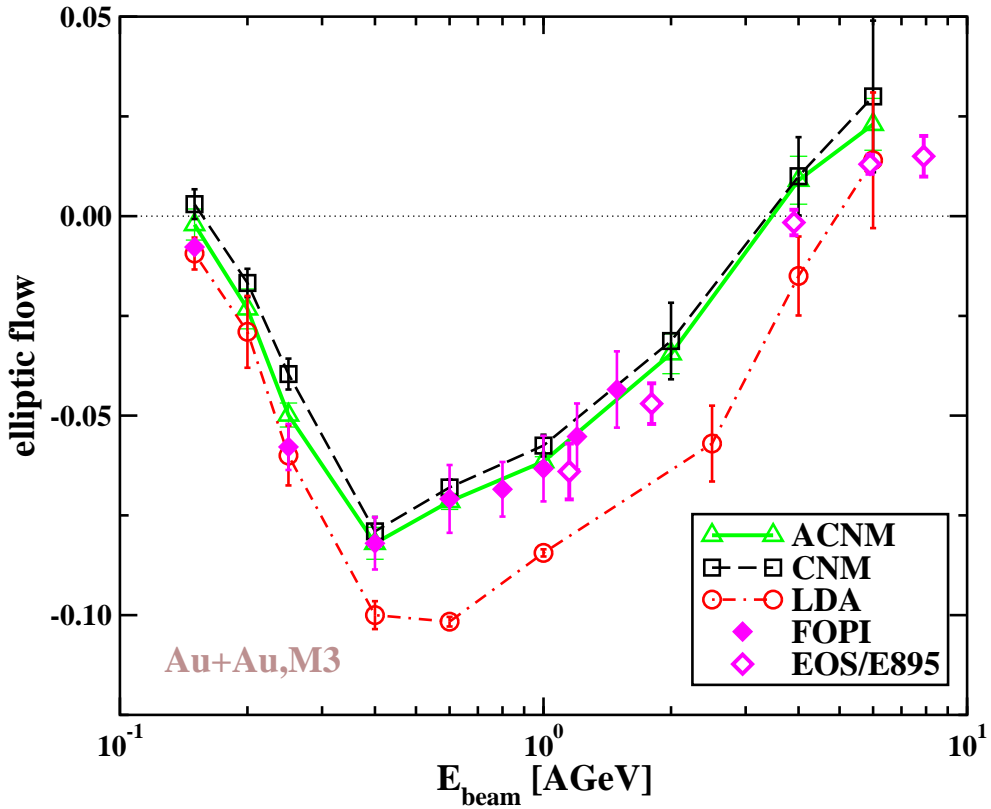


Fig. 7. The excitation function of the elliptic flow v_2 in peripheral Au+Au collisions obtained with the models of Fig. 4, see also [24]. The data (open and filled diamonds) are taken from [14,23].

References

- [1] W. Reisdorf, H.G. Ritter, *Annu. Rev. Nucl. Part. Sci.* **47** (1997) 663; N. Hermann, J.P. Wessels, T. Wienold, *Annu. Rev. Nucl. Part. Sci.* **49** (1999) 581, and references therein.
- [2] C. Fuchs, P. Essler, T. Gaitanos, H.H. Wolter, *Nucl. Phys.* **A626** (1997) 987.
- [3] F. Rami, Y. Leifels, *et al.* (FOPI-Kollaboration), *Phys. Rev. Lett.* **84** (2000) 1120.
- [4] P. Danielewicz, *Nucl. Phys.* **A673** (2000) 375.
- [5] P.K. Sahu, A. Hombach, W. Cassing, M. Effenberger, U. Mosel, *Nucl. Phys.* **A640** (1998) 493.
- [6] W. Botermans and R. Malfliet, *Phys. Rep.* **198** (1990) 115.
- [7] L. Sehn, H.H. Wolter, *Nucl. Phys.* **A601** (1996) 473.
- [8] C. Fuchs, T. Gaitanos, *Nucl. Phys.* **A714** (2003) 643.
- [9] C. Fuchs, T. Gaitanos, H.H. Wolter, *Phys. Lett.* **B381** (1996) 23; T. Gaitanos, C. Fuchs, H.H. Wolter, *Nucl. Phys.* **A650** (1999) 97.
- [10] T. Gaitanos, C. Fuchs, H.H. Wolter, A. Faessler, *Eur. Phys. J.* **A12** (2001) 421.
- [11] B. ter Haar, R. Malfliet, *Phys. Rep.* **149** (1987) 207; *Phys. Rev.* **C36** (1987) 1611.
- [12] T. Gross-Boelting, C. Fuchs, and A. Faessler, *Nucl. Phys.* **A648** (1999) 105.
- [13] J. Cugnon *et al.*, *Nucl. Instr. and Meth. in Phys. Res.* **B111** (1996) 215; H. Huber, J. Aichelin, *Nucl. Phys.* **A573** (1994) 587.
- [14] C. Pinkenburg *et al.* (E895 Collaboration), *Phys. Rev. Lett.* **83** (1999) 1295.
- [15] Ch. Hartnack *et al.*, *Eur. Phys. J.* **A1** (1998) 151.
- [16] S.A. Bass, M. Belkacem, M. Bleicher *et al.*, *Prog. Part. Nucl. Phys.* **41** (1998) 225.
- [17] B.A. Li *et al.*, *Phys. Rev.* **C60** (1999) 011901.
- [18] Y.M. Zheng *et al.*, *Phys. Rev. Lett.* **83** (1999) 2534.
- [19] B. Blaettel, V. Koch, U. Mosel, *Rep. Prog. Phys.* **56** (1993) 1.
- [20] P. Danielewicz *et al.*, *Phys. Rev. Lett.* **81** (1998) 2438.
- [21] P. Crochet, F. Rami, R. Dona *et al.* (FOPI-Kollaboration), *Nucl. Phys.* **A627** (1997) 522; P. Crochet, F. Rami, J.P. Coffin *et al.* (FOPI-Kollaboration), in XXXIV International Winter Meeting of Nuclear Physics, Bormio, Italy, 1996, ed. I.

Iori, Univ. di Milano.;

N. Bastid, A. Buta, P. Crochet *et al.* (FOPI–Kollaboration), *Nucl. Phys.* **A622** (1997) 573.

[22] A. Andronic, W. Reisdorf, N. Hermann et al. (FOPI collaboration), *Phys. Rev. C* **66** (2003) 034907.

[23] A. Andronic (FOPI collaboration), private communication.

[24] We have repeated the calculations for the elliptic flow excitation function for peripheral Au+Au reactions up to 1 AGeV to achieve results with more precise statistics. The theoretical calculations of Fig. 7 with the LDA and CNM mean fields only slightly differ from those already published in [8].

[25] P. Danielewicz, *Acta. Phys. Pol.* **B33** (2002) 45.

A Appendix

The ACNM configuration (1) given by two counterstreaming nuclear matter currents is characterized by three parameteres, namely the Fermi momenta $k_{F_{1,2}}$, respectively the rest densities of the currents, and their relative velocity v_{rel} . Expression (1) contains a Pauli correction term $\delta f = -\Theta_1\Theta_2$ which restores the Pauli principle in case that the relative velocity of the currents is small and the original ellipsoids overlap. As discussed in detail in [7] the Pauli correction can be performed in a covariant way. Corresponding expressions for the Pauli correction terms can be found in [7].

In [7] the mean field, respectively the counterstreaming self-energy components have been derived for symmetric nuclear matter configurations ($k_{F_1} = k_{F_2}$). Here we present the extension to the general case of asymmetric configurations ($k_{F_1} \neq k_{F_2}$). In order to obtain mean fields in a Hartree form which depend only on the ACNM parameters $\{k_{F_{1,2}}, v_{\text{rel}}, \rho_\delta\}$ the self energy contributions of the two currents $\Sigma_m^{(i)}$, ($i = 1, 2, \delta, m = s, 0$) have to be averaged over the ACNM configuration in momentum space. This includes also corrections arising from the conservation of the Pauli principle.

Since the underlying DB self-energies show only a moderate momentum dependence below the Fermi surface ($k \leq k_F$) [12] the integrations over the comoving current and also over the overlapp region are numerically easy to carry out due to moderate relative momenta. The difficulty appears for the remaining integrations of the self-energies over the second Fermi ellipsoid ($i \neq j$)

$$\int \Sigma_m^{(i)} f_j$$

It is convinient to perform the integrations of the self energies $\Sigma_m^{(i)}$ in their corresponding rest frames RS_i . In this frame they depend only on the modulus of the 3-momentum which reduces the integrations (in polar coordinates) to two dimensions. In particular, one has to perform integrations over spherical cells which include the integration area over the second ellipsoid as schematically depicted in Fig. A.1.

Let us for example consider the integration of $\Sigma_s^{(1)}|_{RS_1}$ over the other ellipsoid S_2 , which has to be performed in the rest frame RS_1 (Fig. A.1 with $i=1, j=2$):

$$\mathcal{C} \int d^3k \Gamma_{s1}(k_{F_1}, k) f_2 \frac{m^*}{E^*} = m^* \mathcal{C} \int_{k_{min}}^{k_{max}} k^2 dk \int_{\Omega(k)} d\Omega(k) \Gamma_{s1}(k_{F_1}, k) f_2 \frac{m^*}{\sqrt{k^2 + m^*}} .$$

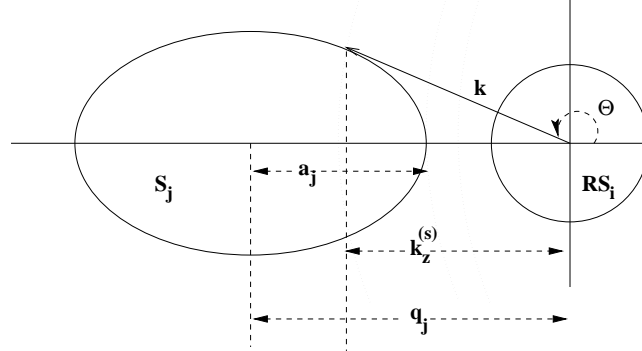


Fig. A.1. Schematic representation of the averaging of the self energies over the ACNM distribution. The integration of $\Sigma_m^{(i)}|_{RS_i}$ has to be performed in the rest frame RS_i by integrating over the other ellipsoid in polar coordinates.

The integration of the spatial angle $\cos \theta = \frac{k_z^{(s)}}{k}$ yields

$$\int_{\Omega(k)} d\Omega(k) = -2\pi \int_{k_z^{(s)}/k}^{-1} = 2\pi \left(-1 - \frac{k_z^{(s)}}{k} \right) .$$

The intersection point $k_z^{(s)}$ of the sphere with radius k_z with the second ellipsoid 2 is thereby given as [7]

$$k_z^{(s)} = \frac{\gamma_1 E_{F_2} - \gamma_2 E_{F_1}}{\gamma_1 \gamma_2 (v_1 - v_2)} . \quad (A.1)$$

Using eq. (A.1) with $v_1 = 0$, $v_2 = -v_{\text{rel}}$, $q_1 = 0$, $\gamma_1 = 1$ und $k_{F_1} = k$ one obtains

$$k_z^{(s)}|_{RS_1} = \frac{E_{F_2} - \gamma(v_{\text{rel}}) \sqrt{k^2 + m^{*2}}}{\gamma(v_{\text{rel}}) v_{\text{rel}}} .$$

In summary the integration over the polar angles leads to

$$\Omega(k) = \begin{cases} 2\pi \left[1 + \frac{1}{v_{\text{rel}} k} \left(\frac{E_{F_2}}{\gamma} - \sqrt{k^2 + m^{*2}} \right) \right] \text{ in } RS_1 \\ 2\pi \left[1 + \frac{1}{v_{\text{rel}} k} \left(\frac{E_{F_1}}{\gamma} - \sqrt{k^2 + m^{*2}} \right) \right] \text{ in } RS_2 \end{cases} .$$

In general, there exist different cases depending on the position of the center of the ellipsoid S_j , i.e. it can lie inside or outside the sphere with radius k . This leads to different cases for the integration $\int d\Omega$:

$$\begin{aligned}
S_j \text{ outside of } RS_i &= \begin{cases} |q_j| - a_j < k < |q_j| + a_2 \int d\Omega(k) = 2\pi(1 + k_z^{(s)}/k) \\ \text{otherwise} \end{cases} \\
S_j \text{ inside } RS_i &= \begin{cases} 0 \leq k \leq a_j - |q_j| & \int d\Omega(k) = 4\pi \\ a_j - |q_j| < k < a_j + |q_j| \int d\Omega(k) = 2\pi(1 + k_z^{(s)}/k) \\ k \geq a_j + |q_j| & \int d\Omega(k) = 0 \end{cases} \quad (\text{A.2})
\end{aligned}$$

The cases (A.2) can be summarized. For the scalar part of the self energy $\Sigma_s^{(i)}$ the integration over the second ellipsoid S_j in the rest frame RS_i reads

$$\begin{aligned}
m^* \mathcal{C} \int_{k_{min}}^{k_{max}} k^2 dk \frac{\Gamma_{si}(k_{F_i}, k)}{\sqrt{k^2 + m^{*2}}} \cdot \int_{\Omega(k)} d\Omega(k) = \\
2\pi m^* \left\{ \int_0^{\max\{0, a_j - |q_j|\}} \frac{\Gamma_{si}(k_{F_i}, k)}{\sqrt{k^2 + m^{*2}}} 2k^2 dk + \right. \\
\left. \int_{|a_j - |q_j||}^{a_j + |q_j|} \frac{\Gamma_{si}(k_{F_i}, k)}{\sqrt{k^2 + m^{*2}}} \left[k^2 + \frac{k}{v_{rel}} \left(\frac{E_{F_j}}{\gamma} - \sqrt{k^2 + m^{*2}} \right) \right] dk \right\} \quad .
\end{aligned}$$

The total scalar part of the ACNM self energy averaged over the ACNM configuration reads finally

$$\begin{aligned}
\bar{\Sigma}_s^{(12)}(\chi) \rho_s^{(12)}(\chi) &= \left\{ \Gamma_{s1}(k_{F_1}) \rho_s^{(1)2}(\chi) + \Gamma_{s2}(k_{F_2}) \rho_s^{(2)2}(\chi) + \right. \\
2\pi m^* \mathcal{C} \left[\int_0^{\max[0, \gamma(k_{F_1} - v_{rel}E_{F_1})]} \frac{\Gamma_{s2}(k_{F_2}, k)}{\sqrt{k^2 + m^{*2}}} 2k^2 dk + \right. \\
\left. \left. \int_{\gamma|k_{F_1} - v_{rel}E_{F_1}|}^{\gamma(k_{F_1} + v_{rel}E_{F_1})} \frac{\Gamma_{s2}(k_{F_2}, k)}{\sqrt{k^2 + m^{*2}}} \left(k^2 + \frac{k}{v_{rel}} \left(\frac{E_{F_1}}{\gamma} - \sqrt{k^2 + m^{*2}} \right) \right) dk \right] \cdot \rho_s^{(2)}(\chi) + \right. \\
2\pi m^* \mathcal{C} \left[\int_0^{\max[0, \gamma(k_{F_2} - v_{rel}E_{F_2})]} \frac{\Gamma_{s1}(k_{F_1}, k)}{\sqrt{k^2 + m^{*2}}} 2k^2 dk + \right. \\
\left. \left. \int_{\gamma|k_{F_2} - v_{rel}E_{F_2}|}^{\gamma(k_{F_2} + v_{rel}E_{F_2})} \frac{\Gamma_{s1}(k_{F_1}, k)}{\sqrt{k^2 + m^{*2}}} \left(k^2 + \frac{k}{v_{rel}} \left(\frac{E_{F_2}}{\gamma} - \sqrt{k^2 + m^{*2}} \right) \right) dk \right] \cdot \rho_s^{(1)}(\chi) + \right. \\
\left. 2\delta \rho_s(\chi) \sum_{j=1,2} \Gamma_{sj}(k_{F_j}) \rho_s^{(j)}(\chi) + \Gamma_s(\min(k_{F_1}, k_{F_2})) \delta \rho_s^2(\chi) \right\} \quad (\text{A.3})
\end{aligned}$$

The scalar densities depend on the ACNM parameters χ due to the configuration dependence of the effective mass $m^* = m^*(\chi)$. The determination of the vector part of the mean field can be performed in a similar way. First one defines it covariantly by

$$\begin{aligned}\bar{\Sigma}^{(12)\mu}(\chi) &= \mathcal{C} \int d^3k \Sigma^{(12)\mu}(k; \chi) f_{12}(k; \chi) \frac{k^\nu}{E} j_{12\nu} / j_{12\alpha} j_{12}^\alpha \\ &= \langle \Sigma^{(12)\mu}(k; \chi) f_{12}(k; \chi) \frac{k^\nu}{E} \rangle j_{12\nu} / j_{12\alpha} j_{12}^\alpha \\ &\equiv T_{vec}^{\mu\nu} j_{12\nu} / j_{12\alpha} j_{12}^\alpha \quad ,\end{aligned}\quad (\text{A.4})$$

with $T_{vec}^{\mu\nu} \equiv \langle \Sigma^{(12)\mu} f_{12} k^\nu / E \rangle$. Eq. (A.4) is valid in any reference frame, hence also in the special frame $RS12$ where the total baryon current vanishes:

$$\begin{aligned}\bar{\Sigma}^{(12)\mu} \equiv T_{vec}^{\mu\nu} j_{12\nu} / j_{12\alpha} j_{12}^\alpha &= \left[\Gamma_{01} j_1^\mu j_1^\nu + \Gamma_{02} j_2^\mu j_2^\nu + \bar{\Gamma}_{02}^1 j_1^\mu j_2^\nu + \bar{\Gamma}_{01}^2 j_2^\mu j_1^\nu + \right. \\ &\quad \left. \Gamma_{01} (j_1^\mu \delta j^\nu + \delta j^\mu j_1^\nu) + \Gamma_{02} (j_2^\mu \delta j^\nu + \delta j^\mu j_2^\nu) + \right. \\ &\quad \left. \Gamma_{0\delta} \delta j^\mu \delta j^\nu \right] j_{12\nu} / j_{12\alpha} j_{12}^\alpha \quad .\end{aligned}\quad (\text{A.5})$$

Here Γ_{0i} contains the integration over the comoving ellipsoid RS_i , and $\bar{\Gamma}_{0i}^j$ denotes the corresponding integration over the second ellipsoid j . These are exactly the same integrations as discussed above.

From the averaged self energies (A.3,A.5) one can finally derive effective coupling functions for the ACNM configuration according to Eq. (6) with $m \equiv s, 0$

$$\bar{\Gamma}_m^{(12)}(\chi) = \frac{\bar{\Sigma}_m^{(12)}(\chi)}{\rho_m^{(12)}(\chi)} \quad .\quad (\text{A.6})$$